Available online at www.sciencedirect.com
ScienceDirect
Journal of Power Sources 159 (2006) 560–569
JOURNAL OF POWER SOURCES
www.elsevier.com/locate/jpowsour

On the influence of temperature on PEM fuel cell operation

M. Coppo [a,*], N.P. Siegel [b], M.R. von Spakovsky [c]

[a] *Energy Engineering Department, Politecnico di Torino, Corso Duca Degli Abruzzi 24, Torino 10129, Italy*
[b] *Sandia National Laboratories, P.O. Box 5800, Albuquerque, NM 87185-0753, USA*
[c] *Center for Energy Systems Research, Mechanical Engineering Department, Virginia Polytechnic Institute and State University, Blacksburg, VA 24061, USA*

Received 14 September 2005; accepted 30 September 2005
Available online 27 December 2005

Abstract

The 3D implementation of a previously developed 2D PEMFC model [N.P. Siegel, M.W. Ellis, D.J. Nelson, M.R. von Spakovsky, A two-dimensional computational model of a PEMFC with liquid water transport, J. Power Sources 128 (2) (2004) 173–184; N.P. Siegel, M.W. Ellis, D.J. Nelson, M.R. von Spakovsky, Single domain PEMFC model based on agglomerate catalyst geometry, J. Power Sources 115 (2003) 81–89] has been used to analyze the various pathways by which temperature affects the operation of a proton exchange membrane fuel cell [M. Coppo, CFD analysis and experimental investigation of proton exchange membrane fuel cells, Ph.D. Dissertation, Politecnico di Torino, Turin, Italy, 2005]. The original model, implemented in a specially modified version of CFDesign® [CFDesign® V5.1, Blue Ridge Numerics, 2003], accounts for all of the major transport processes including: (i) a three-phase model for water transport in the liquid, vapor and dissolved phases, (ii) proton transport, (iii) gaseous species transport and reaction, (iv) an agglomerate model for the catalyst layers and (v) gas phase momentum transport. Since the details of it have been published earlier [N.P. Siegel, M.W. Ellis, D.J. Nelson, M.R. von Spakovsky, A two-dimensional computational model of a PEMFC with liquid water transport, J. Power Sources 128 (2) (2004) 173–184; N.P. Siegel, M.W. Ellis, D.J. Nelson, M.R. von Spakovsky, Single domain PEMFC model based on agglomerate catalyst geometry, J. Power Sources 115 (2003) 81–89; N.P. Siegel, Development and validation of a computational model for a proton exchange membrane fuel cell, Ph.D. Dissertation, Virginia Polytechnic Institute and State University, Blacksburg, VA, 2003], only new features are briefly discussed in the present work. In particular, the model has been extended in order to account for the temperature dependence of all of the physical properties involved in the model formulation. Moreover, a novel model has been developed to describe liquid water removal from the gas diffusion layer (GDL) surface by advection due to the interaction of the water droplets and the gas stream in the gas flow channels (GFC). The complete cell model has been validated against experimentally measured polarization curves, showing good accuracy in reproducing cell performance over a wide range of operating temperatures and making it possible to use the model to study the effect of temperature-dependent parameter variations on cell performance. An important conclusion of the study found that both liquid water transport within the GDL and liquid water removal from the surface of the GDL play a crucial role in determining variations in cell performance with temperature.

Keywords: PEM fuel cell; Temperature effect; Mathematical model

1. Introduction

The proton exchange membrane fuel cell has been the subject of an ever-increasing number of modelling efforts for the past 15 years. Undoubtedly, this growing interest has been caused by increasing concerns about pollution and possible anthropogenic global warming and the consequent research for alternative energy systems that could satisfy the energy demands in a cleaner way, such as those based on hydrogen. Because hydrogen must be produced from other chemical species, the devices that use it to generate electric power must be highly efficient in order to make the entire process energy and cost effective. Accurate numerical models represent a powerful tool for improving fuel cell design, and they have been growing in complexity and accuracy as cheap computational power and better cell understanding has become available.

Abbreviations: CCL, cathode catalyst layer; GDL, gas diffusion layer; GDP, gas diffusion parameter; GFC, gas flow channel; MEA, membrane electrode assembly; PEMFC, proton exchange membrane fuel cell

* Corresponding author. Tel.: +39 0161 226 371; fax: +39 0161 266 322.
E-mail address: marco.coppo@polito.it (M. Coppo).

0378-7753/$ – see front matter © 2005 Elsevier B.V. All rights reserved.
doi:10.1016/j.jpowsour.2005.09.069

Nomenclature

Symbol

A	electrode active area ($l\,mm^{-1}$)
c	molar concentration ($mol\,mm^{-3}$)
C_D	drag coefficient
D	diffusion coefficient ($mm^2\,s^{-1}$)
F	Faraday's constant ($C\,mol^{-1}$)
j	volumetric/exchange current density ($A\,mm^{-3}$)
J	superficial current density ($A\,mm^{-2}$)
K	hydraulic permeability (mm^2)
L	length (mm)
R	universal gas constant ($J\,mol^{-1}\,K^{-1}$)
s	pore saturation
S	volumetric source term ($g\,mm^{-3}\,s^{-1}$)
T	temperature (K)
u	velocity ($mm\,s^{-1}$)
w	mass fraction
We	Weber number

Greek letter

α	charge transfer coefficient
ε	porosity
γ	concentration ratio exponent
η	overpotential (V)
λ	membrane water content
ν	kinematic viscosity ($mm^2\,s^{-1}$)
$\prod$	diffusion effectiveness
θ	water contact angle (rad)
ρ	density ($g\,mm^{-3}$)
σ	conductivity ($S\,mm^{-1}$)
τ	tortuosity
ψ	liquid-to-gas velocity ratio
Σ	surface tension ($\mu N\,mm^{-1}$)

Subscript

c	cathode
H_2O	water
i	ionic
l	liquid
O_2	oxygen
s	saturation
0	reference value

Superscript

eff	effective
l	liquid
p	polymer
ref	reference

A number of one- and two-dimensional computational models were developed [6–12] but, although they represent significant advances in fuel cell modelling, it has been shown [3] that transport processes occurring in a PEM fuel cell are intrinsically three-dimensional. As a result, it is not possible to accurately predict cell performance unless a realistic, 3D description of the cell geometry is considered. Two-dimensional models are inadequate because they only consider areas where cell efficiency is the largest, thus, strongly overestimating the limiting current unless heavy model tuning is performed. Obviously, this impedes their use as design tools.

Moreover, most models do not include the description of the two-phase flow that takes place in the gas distributor channels. However, the advective removal of liquid water from the GDL surface has been shown to affect the saturation level of the gas diffusion electrode [3], thus, strongly affecting mass transport related voltage losses. Physical properties of electrodes and gas species and their dependence on temperature also significantly affect cell performance. Probably for this reason, most works presenting cell models, even three-dimensional ones [13,14], show comparisons between experimentally measured and numerically obtained data for only one temperature level.

In the present work, a three-dimensional model of a proton exchange membrane fuel cell was used to investigate the effect of operating temperature on cell performance. The model includes a description of two-phase flow in the gas flow channels along with physical property temperature dependencies.

2. Mathematical model development

In order to obtain a fully three-dimensional implementation of the cell model previously developed [1,2], an adequate description of the water removal process occurring at the interface between the GDL and GFC was required. For this reason, a means for calculating the liquid water velocity field in the gas distributor channels without solving a second momentum conservation equation was devised. It was assumed that, in terms of direction, both phases shared the same velocity field but had different magnitudes (i.e. the liquid phase could move slower than the gas phase). Furthermore, a simple mechanical model was used to evaluate the interaction between the gas stream and the liquid water droplets at the GDL/GFC interface. The model uses one of two types of transport processes depending on the flow regime. When the flow surrounding the droplet is laminar, no transverse velocity is present. In this regime, water droplets move along the GDL surface as a result of forces acting on the droplets due to viscous drag and surface tension. The viscous drag and surface tension forces can be expressed in terms of the droplet diameter, drag coefficient, gas and liquid velocity, surface tension and the contact angle. An expression for the ratio of the liquid phase and gas phase velocities can then be obtained by imposing mechanical equilibrium on the forces acting on the droplet. This expression is called the advection coefficient, ψ, and has the form:

$$\psi = 1 - 2\sqrt{\frac{2\,\sin\theta}{We\,C_D}} \tag{1}$$

where the contact angle (θ), drag coefficient and Weber number depend on, or contain properties that depend on temperature. The last two terms are also functions of gas velocity, which varies with temperature for constant mass flow rate conditions, while the water contact angle was shown to be temperature-

dependent in tests carried out at the Politecnico di Torino [3] using digital image analysis techniques. It was found that for the GDL material (E-TEK[1] ELAT HT 1400-W) used in MEA fabrication at Virginia Tech, the following correlation relating temperature to contact angle held:

$$\theta = -0.9444\left(\frac{T}{T_0}\right) + 3.422 \quad (2)$$

where $T_0 = 298$ K and the contact angle is expressed in radians.[2]

When the droplet on the GDL surface is exposed to turbulent flow, it is assumed that local gas phase velocity fluctuations are sufficient to dislodge the droplet from the GDL surface. In the absence of a surface tension force to balance the viscous drag, the droplet accelerates until it reaches the gas phase velocity. Under these conditions the advection coefficient ψ approaches unity.

Having defined the liquid phase velocity field, it is possible to solve the liquid water transport equation in all of the regions of the fuel cell. The transport equation for liquid water is solved in terms of the liquid water saturation, which is the ratio of the local liquid water volume to local pore volume. The mathematical model is completed with the addition of a series of closure relations, which include a correlation for the flow of liquid water by capillary action through the porous media (represented as a diffusive process although it is in fact advective) as well as relations for physical properties such as density, viscosity and surface tension. The electrochemical characteristics of carbon supported platinum electrodes with a Nafion electrolyte were obtained from [15] for several temperature levels.

3. Experimental setup and model validation

The cell used to obtain experimental data for model validation had a single pass serpentine flow field and an active area of 5 cm^2. A three-dimensional computational domain was defined by neglecting the bends in the serpentine channel while preserving the total length, as shown in Fig. 1. An MEA was fabricated and tested to characterize its performance at different temperatures and gas inlet conditions as well as to evaluate certain geometric and physical properties. The mathematical model was then validated experimentally and some of the results of the validation process are summarized in Fig. 2, which shows a series of polarization curves taken over a range of temperatures. The predicted curves are in good agreement with experimental data across the entire operating range. Furthermore, it should be noted that, once the model was tuned for the base case conditions ($T = 333$ K), it was not adjusted further, i.e. no 'knobs' were turned in order to match the experimental data at other temperature levels. A similar figure showing good agreement between predicted and experimental changes in performance due to variations in cathode inlet relative humidity is given in [3]. These validation cases serve to establish confidence in the ability of the model to accurately predict the performance of the test cell under a variety of conditions, making it possible to use the model as a design tool and as a means of studying the effects that contribute to cell performance and how these effects are related to cell temperature.

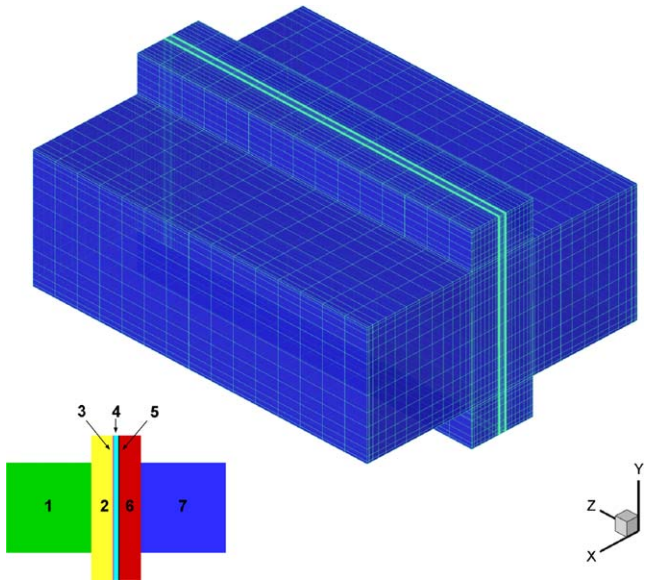

Fig. 1. Three-dimensional computational domain: (1) anode gas channel, (2) anode gas diffusion layer, (3) anode catalyst layer, (4) polymer electrolyte membrane, (5) cathode catalyst layer, (6) cathode gas diffusion layer and (7) cathode gas channel.

In order to emphasize the fact that the phenomena that govern fuel cell operation are intrinsically three-dimensional, and thus, only a 3D model can correctly repoduce them, the same mathematical model was run on both a 2D and a 3D computational domain. From Fig. 3, it is evident that the 2D model greatly overestimates cell performance, since such a model only considers phenomena occurring on a "slice" of cell cut halfway through the channel height. It has been shown [3,5] that this is the region of highest current production and that, departing from it,

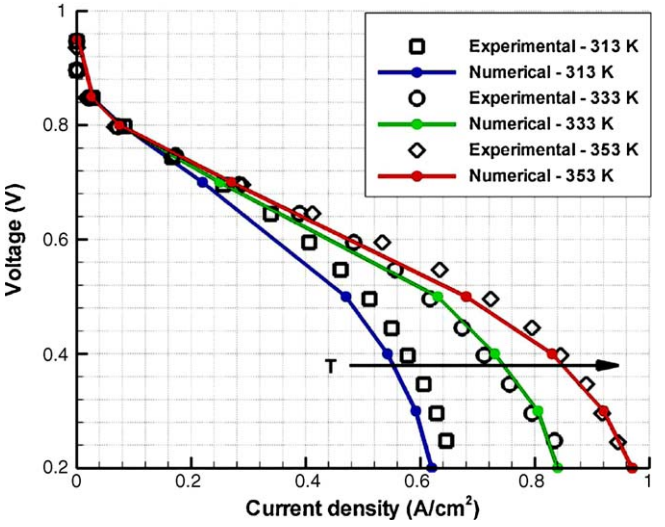

Fig. 2. 3D model validation at different temperature levels.

[1] www.etek-inc.com.

[2] The internal GDL contact angle is assumed to be identical to the surface contact angle at the GDL/GFC interface.

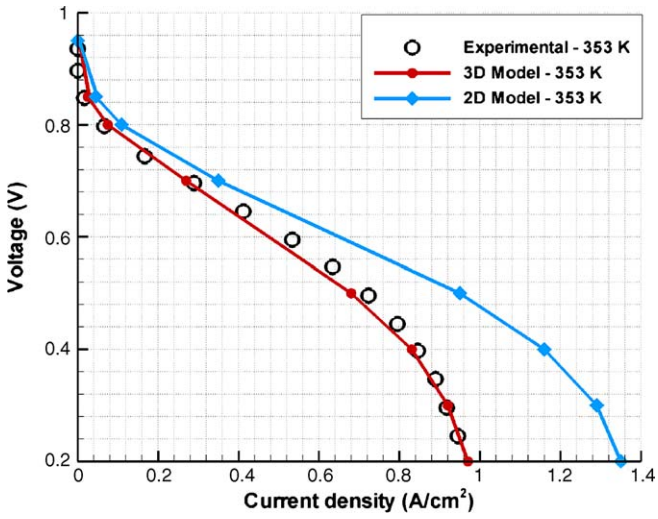

Fig. 3. Effect of three dimensions vs. two dimensions on model predictions.

cell current decreases, especially in the zones under the channel walls. As a result, 2D models fail to correctly estimate cell performance, unless strong parameter tuning is adopted,[3] because such models evaluate performance only at the "best conditions". This, of course, is not the case for well-developed 3D models such as the one used here which quite accurately reproduces the experimental data, as shown in Figs. 2 and 3.

4. Results: temperature effects

As it can be seen from Fig. 2, temperature influences the polarization curve over the entire operating range of the cell. However, as current increases the main cause of voltage loss changes, so that, for low currents, ($0\,A\,cm^{-2} < J < 0.2\,A\,cm^{-2}$) reaction activation losses dominate, in the intermediate range of currents ($0.2\,A\,cm^{-2} < J < 0.7\,A\,cm^{-2}$), ohmic losses are preponderant, and finally, for higher currents, mass transport losses prevail. Furthermore, it follows that temperature influences cell performance in these three regimes to the extent that it affects the leading loss phenomenon. For this reason, in the following discussion, temperature effects on the polarization curve will be studied separately for each operating regime. However, before proceeding, it is useful to recall the relations that describe the physical phenomena that are relevant to this analysis.

The model used here to relate cell current and cathode overpotential (voltage losses) is, essentially, the Butler–Volmer model for reaction kinetics in which an effectiveness term, Π_c, has been introduced. For the cathode catalyst layer:

$$j_c = \Pi_c(1-s)Aj_c^{ref}\left(\frac{c_{O_2}^p}{c_{O_2}^{ref}}\right)^{y_c} \times \left[\exp\left(\frac{\alpha_c F}{RT}\eta_c\right) - \exp\left(-\frac{\alpha_c F}{RT}\eta_c\right)\right] \quad (3)$$

[3] In other words, certain model parameters, such as tortuosity, porosity, kinetic parameters, etc., are arbitrarily modified.

The effectiveness accounts for the resistance to oxygen diffusion posed by the polymer material surrounding the reaction sites within the agglomerate structures of the catalyst layer [2]. An additional term, $(1-s)$, where s represents liquid water saturation, accounts for the deactivation of reaction sites due to local pore flooding. In the following discussion, we will be studying the effect of temperature on each term that appears in Eq. (3), and thus, its effect on cell voltage.

The diffusion characteristics of the porous media do not change with temperature but, because they affect the relative importance of each (temperature-dependent) transport phenomenon, it is interesting to see how temperature effects on the polarization curve change as the porous medium structure does. Thus, in the following analysis, the parameter:

$$\mathrm{GDP} = \frac{\varepsilon}{\tau L}\frac{\tau_0 L_0}{\varepsilon_0} \quad \text{in the GDL} \quad (4)$$

or

$$\mathrm{GDP} = \frac{\varepsilon^{1.5}}{L}\frac{L_0}{\varepsilon_0^{1.5}} \quad \text{in the CCL} \quad (5)$$

is defined and used to characterize the porous media. The gas diffusion parameter (GDP) is a function of porosity (ε), tortuosity (τ) and layer thickness (L). A reference value of GDP, characteristic of the diffusion medium, was used in the experiments as well as a lower one, characteristic of media with worse gas diffusion properties.

Finally, liquid water transport primarily influences cell operation in the high current region of the polarization curve. In the present model, Eq. (6) is used to calculate the distribution of liquid water in the gas channels and porous electrodes. Its solution yields the pore saturation, s:

$$\frac{\partial s}{\partial t} + \vec{\nabla}\cdot(\vec{u}_l s) - \vec{\nabla}\cdot(D_{H_2O}^l \vec{\nabla} s) = \frac{S_s}{\rho_{H_2O}^l} \quad (6)$$

It is worth noting that in porous media the gas phase velocity becomes so small as not to influence the liquid phase, due to the negligible amount of momentum exchanged between the phases. Thus, the advective term drops off, as water flow is driven by capillary pressure only. At these conditions, it is possible to treat this as a diffusive process, defining a suitable diffusion coefficient for liquid water such as:

$$D_{H_2O}^{l(\theta>90^\circ)} = \frac{\Sigma s^3\sqrt{\varepsilon K}\cos\theta}{\nu_{H_2O}^l \rho_{H_2O}^l}(1.417 + 4.240s + 3.789s^2) \quad (7)$$

This was obtained by using Leverett's equation to characterize capillary pressure as a function of saturation so that its diffusivity actually depends on saturation, giving Eq. (6) a non-linear nature.

4.1. Activation regime

In the activation region, cell current density is low so that both mass transport losses due to limited oxygen diffusivity and electrode saturation are negligible. As a result, diffusion effectiveness is also relatively high and constant with temperature. It

Table 1
Activation overpotential dependence on temperature

Temperature (K)	j_c^{ref} (A mm^{-3})	α_c	$w_{O_2}/w_{O_2}^{ref}$	$\eta_c(T)/\eta_c(303)$
303	4.38e−12	0.89	0.069	1.00
313	7.10e−12	0.89	0.068	1.00
323	1.27e−11	0.89	0.066	1.00
333	1.88e−11	0.92	0.062	0.98
343	3.33e−11	0.95	0.056	0.95
353	5.42e−11	0.96	0.047	0.94

Table 2
Ohmic overpotential dependence on temperature

Temperature (K)	$D_{H_2O}^{p}$ (mm^2 s^{-1})	$\sigma_i^{eff}(T)/\sigma_i^{eff}(303)$	$\eta_c(T)/\eta_c(303)$
303	1.30e−4	1.00	1.00
313	1.68e−4	1.15	0.87
323	2.13e−4	1.31	0.76
333	2.67e−4	1.48	0.67
343	3.29e−4	1.66	0.60
353	4.02e−4	1.84	0.54

follows that higher temperature affects the shape of the polarization curve mainly through higher values of both reference exchange current density and charge transfer coefficient, as well as directly by appearing in the exponential part of the reaction kinetics model.

Despite the fact that we can neglect changes in oxygen concentration across the GDL due to low current production, we must take into account the fact that temperature influences the fraction of water in the gas mixture, and thus, that of oxygen. As a result, the concentration-dependent term plays a relevant role in this region too.

By inverting Eq. (3) and considering, for our purposes, a value of current density typical of the activation loss region ($J = 0.05$ A cm^{-2}), one can estimate the cathode activation overpotential variation with temperature. In order to do so, values of electrode properties at various temperature levels are required. These are obtained from [15]. Table 1 presents the results of this analysis in the rightmost column, where the overpotential variation with respect to the reference case (303 K) is reported. As can be seen, temperature causes an increase in kinetic parameters, while it reduces the concentration term, because the oxygen mass fraction decreases at higher temperatures, as more water is present in the gas mixture. The increase in kinetics somewhat offsets the reduction in oxygen concentration, so that the net result is a decrease of the cathode activation overpotential with temperature. In terms of cell performance, this is desirable because lower ovepotentials result in higher cell voltage (and thus, efficiency). However, this effect is mitigated somewhat by the fact that the open circuit voltage decreases for higher values of temperature.

4.2. Ohmic regime

In the ohmic region of the polarization curve, the total cathode overpotential is primarily a result of ohmic losses in the membrane, particularly on the anode side, due to membrane dryout caused by electro-osmotic drag. As a result, the temperature-dependent, loss-controlling parameters in this region are membrane ionic conductivity and dissolved water diffusivity. The latter influences the former because, for the same current density, a higher diffusivity implies a more uniform dissolved water distribution, thus, eliminating zones of very low conductivity.

In order to study how these temperature-dependent properties affect ohmic losses in the cell, let us consider that the electro-osmotic drag is mainly dependent on current density. Hence, for a given value of current density, it follows from the dissolved water transport equation that the water content gradient will increase as the relative diffusion coefficient decreases. Thus, by solving this equation, one obtains the polymer water content profiles for each temperature level. With this, one can estimate membrane conductivity, and ultimately, ohmic overpotential. Table 2 presents the results of this analysis, obtained by applying the procedure defined above and simulating cell operation at 0.5 A cm^{-2}.

The results clearly show the benefits of higher operating temperatures when the cell is working in the ohmic region of its polarization curve, because the portion of the open circuit voltage lost to driving the flow of ions almost halved when increasing the temperature from 303 to 353 K. The reason behind this can be more effectively understood by looking at Fig. 4. It is clear that membrane conductivity increases not only because of its own dependence upon temperature [16], but also because the increased diffusion coefficient of dissolved water (which, for a given membrane, is mainly function of temperature, as shown in Fig. 4) allows a more uniform distribution of water in the membrane, and thus, eliminates zones of high resistance to ion transport. In addition, the ability of the membrane to uptake water increases with temperature, which leads to a greater overall water content and a corresponding increase in ionic conductivity.

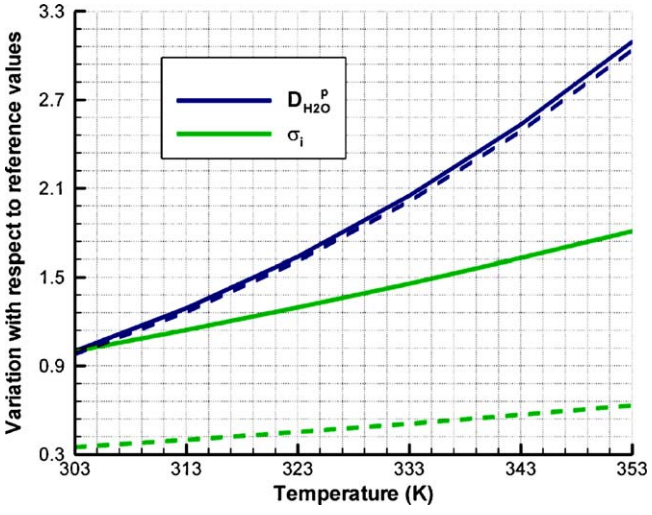

Fig. 4. Temperature dependence of dissolved water diffusivity and membrane ionic conductivity; continuous lines were obtained with a reference value of membrane water content ($\lambda = 16$) while dashed lines show the effect of a 50% reduction in λ on the same variables.

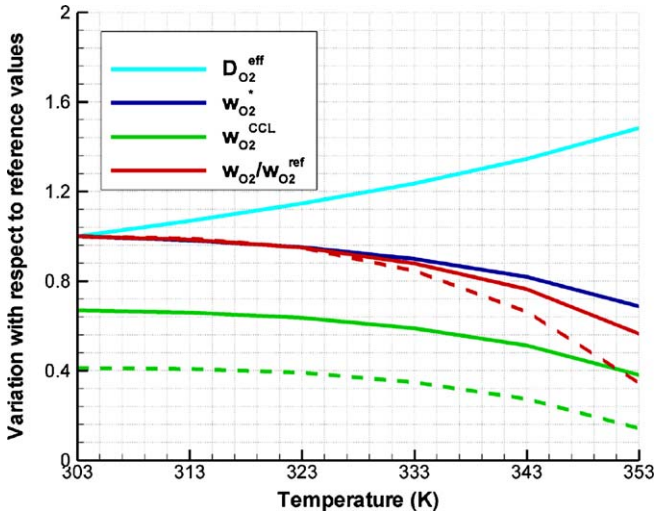

Fig. 5. Temperature dependence of oxygen mass fraction and diffusivity for oxygen diffusion in both the GDL and CCL; continuous lines are based on a reference value of GDP while dashed lines are based on a 44% reduction in GDP.

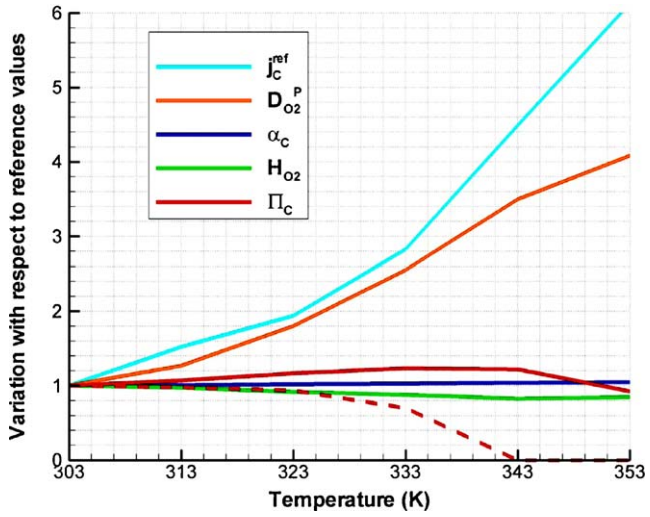

Fig. 6. Temperature dependence of kinetic and diffusion-in-polymer parameters; as before, since effectiveness depends on GDP, two trends are reported: continuous lines based on a reference value of GDP and dashed lines based on a 44% reduction in GDP.

4.3. Mass transport limited regime

In the mass transport limited region, in addition to ohmic and activation losses, cell voltage is strongly affected by resistance to reactant transport, given the high mass flow rate required to sustain the electrochemical reactions at such a high rate. Temperature effects on this region, and in particular, on the limiting current, are some of the most difficult to explain because of the many phenomena that interact with and influence each other at high current density. In order to understand the mechanisms by which temperature influences limiting current, its influence on each phenomenon and parameter affecting maximum current density was analyzed.

4.4. Oxygen transport

Oxygen transport limitations affect the limiting current due to the diffusion resistance of the GDL, since the flow rate necessary to produce an ever higher current[4] is generated by increasing the concentration gradient across the GDL, assuming, of course, that the fraction of oxygen at the channel inlet is fixed. Oxygen mass transport becomes limiting with respect to the reaction rate when its concentration reaches very small values in the catalyst layer. The current at which this happens depends on the oxygen diffusion resistance and the initial value of concentration at the cell inlet, both of which are temperature-dependent.

As can be seen in Fig. 5, oxygen diffusivity increases with temperature. The GDP does not affect the relative change of this parameter with temperature, because porosity, tortuosity and GDL thickness do not vary with temperature, and the dependence upon saturation has been removed in order to study oxygen transport only. In this same figure, the actual-to-reference mass fraction ratio is both temperature- and GDP-dependent since, with fully humidified gases, the higher the temperature is, the higher the water vapor mass fraction and the lower the oxygen value while the lower the GDP is, the lower the oxygen effective diffusion coefficient and consequently the lower the oxygen concentration in the CCL. Fig. 5 presents two trends of the oxygen mass fraction in the CCL and the ratio of mass fractions appearing in the Butler–Volmer equation, because these quantities also depend on GDP. The continuous lines refer to quantities evaluated using the reference value of GDP, while the dashed lines demonstrate the effect of a reduction of GDP on these variables. Furthermore, the reported value of oxygen mass fraction in the CCL was divided by the value at the channel inlet. Thus, one can see that *in the absence of liquid water* in the electrodes, despite the increase in oxygen diffusivity with temperature, the concentration ratio that influences reaction kinetics decreases with temperature. The reason is that the beneficial effects of higher temperature on diffusivity are offset by the detrimental ones due to higher water content in the gas stream, and thus reduced oxygen concentration at the cell inlet.

4.5. Kinetic parameters

The temperature effects on reaction kinetic parameters such as the reference exchange current density (j^{ref}), the charge transfer coefficient (α) and the diffusion effectiveness (Π) are shown in Fig. 6.[5] Little change in the transfer coefficient is observed while exchange current density shows a 6-fold increase in the range of 303–353 K. The behavior of the effectiveness is interesting because its trend changes based on the GDP. This is explained by the fact that, if GDP is high, then the oxygen

[4] For this study, temperature effects on mass transport are evaluated at a fixed cell current density of 0.8 A cm^{-2}.

[5] Fig. 6 also shows an increase in effective O_2 diffusivity in the polymer of the agglomerates, while O_2 solubility (Henry's constant) slightly decreases. The effective diffusivity is the product of these two quantities and increases.

concentration remains relatively high in the catalyst layer even at high temperatures due to modest gradients, since the controlling diffusion phenomenon (i.e. the one showing the highest resistance) becomes oxygen transport in the polymer of the agglomerate. The result is a higher effectiveness. However, after a certain temperature threshold (343 K in the above figure), oxygen transport in the gas phase is so affected by the reduced inlet mass fraction that effectiveness again decreases. A discussion of how the temperature dependence of oxygen transport and reaction kinetics affects cathode overpotential, and consequently, cell voltage, is reported in [3].

4.6. Liquid water transport

In what has been presented to this point, liquid water in the electrode (GDL/CCL) has so far been neglected. However, it does play a significant role in determining cell voltage and limiting current. In our model, water transport in the porous media has been modelled as capillary pressure driven flow. Thus, it is possible to describe it as a diffusive process by defining a suitable diffusivity in the liquid water transport equation (saturation equation). This diffusivity depends non-linearly on the transported variable (saturation) as well as on surface tension, contact angle, kinematic viscosity and porosity. Thus, studying the effects of only temperature on water transport required splitting the definition of the liquid water diffusivity into a term containing only functions of saturation, and another containing only physical properties. All the latter vary with temperature, and their combined effect on the saturation-independent part of the diffusivity is presented in Fig. 7. It is interesting to note that the trends reported vary according to the value of contact angle used. The green lines (both continuous and dashed) refer to contact angle values, which vary as in Eq. (2) above. The same trend was also shifted down so that the highest value (at lowest temperature) of θ was about 110°. This allowed investigation of the effect on liquid water transport of a less hydrophobic porous medium.

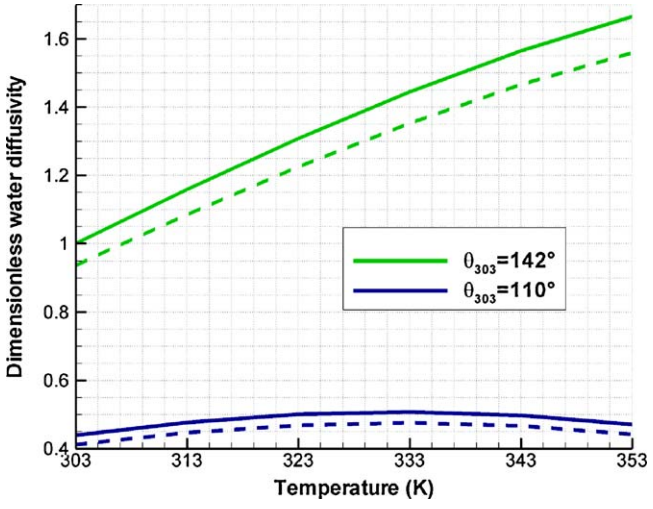

Fig. 7. Liquid water diffusivity dependence upon temperature and contact angle; as before, since the diffusivity depends on GDP, two trends are reported: continuous lines based on a reference value of GDP and dashed lines based on a 44% reduction in GDP.

The result as seen in Fig. 7 is that highly hydrophobic porous materials (the green lines) show values of water diffusivity that monotonically increase within the temperature range considered, while less hydrophobic porous media present a maximum value of diffusivity in the middle of the temperature range. These results show the importance of accurately characterizing the surface properties of diffusion media as the temperature varies.

Now, if one assumes that the liquid water source in the cathode catalyst layer (due to production by reaction, transport by electro-osmotic drag and diffusion through the polymer) does not depend upon temperature,[6] then an increase in the diffusivity is followed by a decrease in the saturation gradient so as to keep the water flux constant. As the temperature rises, contact angle and surface tension decrease as does the kinematic viscosity. The trends reported in Fig. 7 suggest that the latter presents the largest variations, causing the diffusivity to increase so that for a given cell current, the saturation gradient over the GDL decreases. Assuming for the sake of clarity that saturation in the channel equals zero at a short distance from the interface with the GDL, a smaller saturation gradient implies a smaller absolute value in the CCL, which in turn, results in an enhancement of oxygen diffusivity and reaction kinetics at higher temperatures and a detriment of the same properties if temperature is reduced.

Of course, since the liquid water diffusivity is a function of saturation as well, the resulting trend of water content in the pores is non-linear, which means that the actual value of saturation affects its gradient. This, in turn, is a function of water flux into the CCL as well as the flux out of the GDL/gas channel interface. The latter, as mentioned earlier, is defined by the interaction of water droplets with the gas stream in the gas channels and, as shown in [3], can be described as a function of an appropriate advection coefficient with a strong dependence upon temperature, i.e. increasing two orders of magnitude in the range from 333 to 353 K. The result is that the flux out of the GDL is greatly enhanced by an increase in temperature, leading to saturation levels in the GDL which are lower, and in turn benefiting not only oxygen gas diffusion in the pores but in the polymer phase of the agglomerates as well. The result is a greater effectiveness.

Thus, if both reaction kinetics and mass transport effects that include liquid water transport are taken into account when predicting cell behavior, the most noticeable effect is a more pronounced increase in oxygen diffusivity with temperature when no liquid water is present (compare Fig. 8 with Figs. 5 and 6 above). This in turn contributes to an increase of oxygen mass fraction in the CCL over most of the temperature range and an increase in the concentration-dependent term of the Butler–Volmer equation. In contrast, the effect of saturation is to invert the trends (at least for a large part of the temperature

[6] With this assumption we are neglecting temperature induced variations of dissolved water diffusivity, which affect the magnitude of electro-osmotic drag.

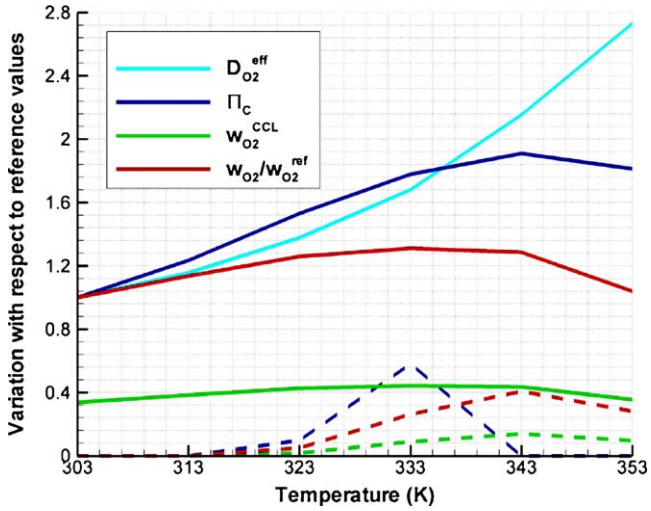

Fig. 8. Temperature dependence of quantities related to oxygen diffusion, affected by the presence of liquid water in the diffusion media; as before, due to GDP dependence, two trends are reported: continuous lines based on a reference value of GDP and dashed lines based on a 44% reduction in GDP.

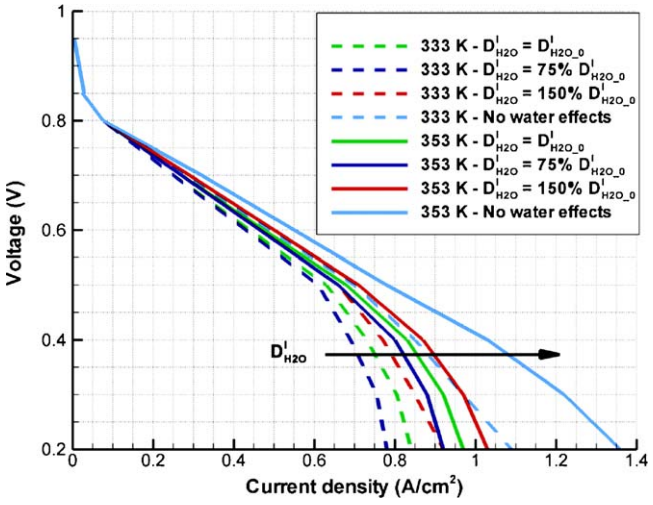

Fig. 9. Effect of liquid water presence in the GDL on cell performance.

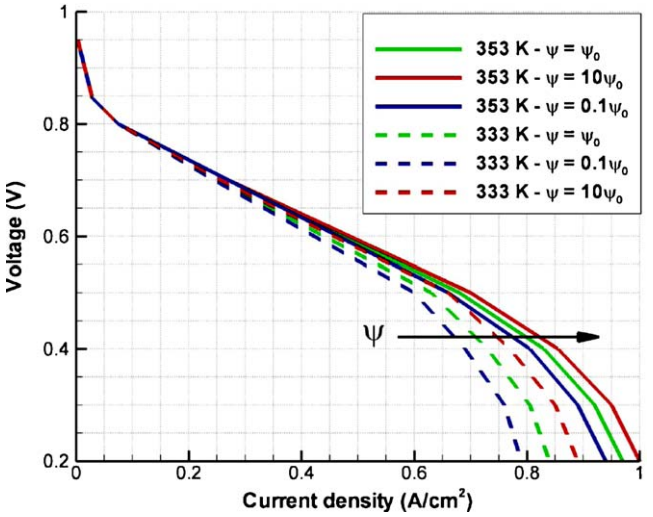

Fig. 10. Effect of advection coefficient on cell performance.

range) seen previously in Figs. 5 and 6 for dry electrodes. Furthermore, comparing the effectiveness curves, one notes that saturation affects oxygen diffusivity in the polymer so strongly as to double the effectiveness in the range from 303 to 343 K, while the dry electrode trends show only a 20% increase. It is also interesting to note that the combined effect of liquid water and lower electrode GDP is that of reducing the oxygen concentration in the CCL, and thus, effectiveness, as well as shifting the peak values of both of these variables to lower temperatures. Thus, as one would expect, at lower temperature and GDP the cell performs badly since as the peak values of oxygen concentration in the CCL and effectiveness shift to lower temperatures as well as lower values, the optimal operating temperature decreases a bit as GDP decreases. This can be explained by the fact that the concentration gradient will be steeper for a lower GDP, and thus, the benefit of starting with higher concentration in the gas channel (which happens at lower temperatures) offsets the decreased ability to get rid of water from the GDL, resulting in a decrease in the value of the optimal operating temperature.

Finally, the effects of liquid water and advection coefficient on fuel cell performance are seen with the polarization curves given in Figs. 9 and 10. The results, for example, in Fig. 9 show that when liquid water diffusivity is reduced by 25% the limiting current decreases by 7.1 and 5.1% at 333 and 353 K, respectively. Conversely, at these same temperatures, when the diffusivity is increased by 50%, the limiting current increases by 9.5 and 6.2%, respectively. These trends can also be analyzed in terms of GDL hydrophobic effects on cell performance. In fact, the required reduction and increase in diffusivity were obtained by varying the contact angle θ, i.e. the 25% reduction in liquid water diffusivity was achieved by reducing the contact angle by 9%, while the 50% increase was obtained by increasing contact angle by 13%.

Fig. 10 shows the effects of changes in the advection coefficient, indicating that these effects are more marked at lower temperatures (±6% at 333 K versus ±3% at 353 K), since water transport inside the GDL is less efficient and the gas velocity is lower.[7] This allows the formation of bigger droplets on the surface of the GDL/gas channel interface and in turn causes saturation to increase in the GDL, reducing reactant diffusivity. The significant effect on polarization seen in this figure demonstrates the need for accurately characterizing two-phase mass transport phenomena at the interface between the gas channel and GDL. Any model that does not is bound to be incomplete, since not only would water removal be incorrectly estimated, but so would the estimation of limiting current and cell performance.

[7] This happens because the stoichiometric ratio and, as a consequence, the dry air mass flow rate, are kept constant for all cell operating conditions. However, different temperature levels require different rates of water uptake in the dry gas stream for complete humidification. Thus, the mass flow rate of the humidified mixture in the channel varies with temperature, as velocity does.

5. Conclusions

The improved liquid water transport model, along with the characterization of physical properties dependence upon temperature and the effects on oxygen diffusion of a catalyst layer made up of agglomerates, has helped obtain a good agreement between model predictions and experimentally measured cell performance over a wide temperature range. This has made it possible to trust our model predictions, and thus, use them to investigate how temperature-dependent parameters affect cell operation. Some of the conclusions drawn from our study include the following:

- Despite its presence in the denominator of the kinetics equation, higher temperature positively affects reaction kinetics by strongly increasing the reference exchange current density and weakly increasing the charge transfer coefficient.
- In the ohmic region of the polarization curve, benefits of running the cell at higher temperature can be explained with the higher membrane ionic conductivity caused both by temperature itself and by an increase in membrane water content as well as the diffusivity of water within the membrane, which results in an increased and more homogeneous membrane hydration level.
- Higher temperatures also enhance oxygen diffusivity both in the GDL pores and in the ion-conducting polymer. However, because hotter air needs to absorb more water vapor to become saturated, the oxygen fraction at the cell inlet is reduced as temperature is increased. This causes the oxygen concentration in the cathode catalyst layer to be lower at higher temperatures, despite the higher diffusivity. If liquid water presence in the cell electrodes is not taken into account, this reduction is found to offset all the beneficial effects of higher temperatures on kinetic parameters, resulting in a cell that shows a decrease in performance at higher temperatures.
- The liquid water diffusion coefficient is coupled to temperature through the kinematic viscosity, contact angle and surface tension, since the values of these properties decrease as the water temperature increases. The level of hydrophobicity of the GDL material affects how liquid water diffusivity changes with temperature, because for slightly hydrophobic materials ($100^\circ < \theta < 110^\circ$), the decrease in contact angle causes its cosine to vary considerably so that in combination with a decrease in surface tension, it counterbalances the decrease in kinematic viscosity, thus, keeping diffusivity practically constant with temperature. However, if a highly hydrophobic material ($135^\circ < \theta < 150^\circ$) is used as in our case, then a reduction in kinematic viscosity prevails at higher temperatures; and the result is a 1.7-fold increase in diffusivity when temperature varies from 303 to 353 K.
- Water removal by advection at the GDL/GC interface is increased at higher temperatures for two reasons. First of all, gas velocity increases with temperature because in order to keep the stoichiometric ratio constant, the dry air mass flow rate is kept constant. This means that at higher temperatures, the higher water vapor content of fully humidified air causes a higher mass flow rate (and thus, velocity) in the bipolar plate channels. The second effect is related to the magnitude of the advection coefficient, ψ. This is strongly temperature-dependent; and it reaches unity at 353 K, because the flow in the channels becomes turbulent, and liquid water is transported as finely dispersed droplets in the gas stream.
- The result of an increased liquid water diffusivity and a higher advective flux out of the GDL is a lower saturation level in the cathode pores. Since both oxygen effective diffusivity and the reaction kinetics increase as the amount of liquid water within the electrode decreases, it can be said that temperature has a significant impact on these parameters as well.
- Oxygen diffusivity, which is already lower for cooler air, is further reduced by high saturation, and further increased at high temperature by low saturation. It follows from our work here that, for a dry electrode, oxygen diffusivity shows a 1.5-fold increase from 303 to 353 K. If liquid water effects are taken into account, then the oxygen diffusivity shows a 2.7-fold increase in the same temperature interval.
- Higher diffusivity causes a lower concentration gradient, which results in a higher concentration of oxygen in the catalyst layer, despite the lower concentration of oxygen in the gas channel at higher temperature. The result of all of these effects is a reduction of the cathode overpotential as temperature increases, thus, increasing the limiting current.

Finally, it should be emphasized that even though the conclusions just listed apply specifically to the PEMFC modelled and experimentally measured here, they are probably nonetheless more broadly applicable, i.e. to, at the very least, other PEMFCs with similar configurations and material characteristics which fall within the range of values considered here. Thus, we believe that our results provide both a qualitative and quantitative basis for drawing needed insights into the behavior of these devices, providing guidance for model development and implementation which can move models similar to ours into the realm of general applicability necessary for their use as design tools.

Acknowledgements

The authors would like to thank Prof. Dongiovanni at the Politecnico di Torino for his technical help with regards to the optical technique used for measuring the contact angle and for his financial support in providing a fast computer at the Politecnico in Italy for our 3D model simulations. Similarly, the authors are grateful to Dr. Schnipke at Blue Ridge Numerics Inc. (BRNI), for providing us with a CFDesign® license and working with us to modify BRNI's commercial code in order to accommodate our fuel cell modelling.

References

[1] N.P. Siegel, M.W. Ellis, D.J. Nelson, M.R. von Spakovsky, A two-dimensional computational model of a PEMFC with liquid water transport, J. Power Sources 128 (2) (2004) 173–184.

[2] N.P. Siegel, M.W. Ellis, D.J. Nelson, M.R. von Spakovsky, Single domain PEMFC model based on agglomerate catalyst geometry, J. Power Sources 115 (2003) 81–89.

[3] M. Coppo, CFD analysis and experimental investigation of proton exchange membrane fuel cells, Ph.D. Dissertation, Politecnico di Torino, Turin, Italy, 2005.
[4] CFDesign® V5.1, Blue Ridge Numerics, 2003.
[5] N.P. Siegel, Development and validation of a computational model for a proton exchange membrane fuel cell, Ph.D. Dissertation, Virginia Polytechnic Institute and State University, Blacksburg, VA, 2003.
[6] D.M. Bernardi, M.W. Verbrugge, A mathematical model of the solid–polymer–electrolyte fuel cell, J. Electrochem. Soc. 139 (9) (1992) 2477–2491.
[7] S. Um, C.Y. Wang, K.S. Chen, Computational fluid dynamics modeling of proton exchange membrane fuel cells, J. Electrochem. Soc. 147 (12) (2000) 4485–4493.
[8] A. Rowe, X. Li, Mathematical modeling of proton exchange membrane fuel cells, J. Power Sources 102 (2001) 82–96.
[9] Z.H. Wang, C.Y. Wang, K.S. Chen, Two-phase flow and transport in the air cathode of proton exchange membrane fuel cells, J. Power Sources 94 (2001) 40–50.
[10] T. Berning, D.M. Lu, N. Djilali, Three-dimensional computational analysis of transport phenomena in a PEM fuel cell, J. Power Sources 102 (2002) 284–294.
[11] W.M. Yan, C.Y. Soong, F. Chen, H.S. Chud, Transient analysis of reactant gas transport and performance of PEM fuel cells, J. Power Sources 143 (2004) 48–56.
[12] Y. Shan, S.Y. Choe, A high dynamic PEM fuel cell model with temperature effects, J. Power Sources 145 (2005) 30–39.
[13] T. Berning, N. Djilali, Three-dimensional computational analysis of transport phenomena in a PEM fuel cell—a parametric study, J. Power Sources 124 (2003) 440–452.
[14] G.H. Guvelioglu, H.G. Stenger, Computational fluid dynamics modeling of polymer electrolyte membrane fuel cells, J. Power Sources 147 (2005) 95–106.
[15] L. Zhang, C. Ma, S. Mukerjee, Oxygen permeation studies on alternative proton exchange membranes designed for elevated temperature operation, Electrochim. Acta 48 (2003) 1845–1859.
[16] T.E. Springer, T.A. Zawodzinski, S. Gottesfeld, Polymer electrolyte fuel cell model, J. Electrochem. Soc. 138 (8) (1991) 2334–2341.